Ab Initio Oligomer Approach to Vibrational Spectra of Polymers: Comparison of Helical and Planar Poly(*p*-phenylene)

Lilee Cuff and Miklos Kertesz*

Department of Chemistry, Georgetown University, Washington, D.C. 20057

Received June 8, 1993; Revised Manuscript Received October 27, 1993®

ABSTRACT: We used the scaled quantum mechanical oligomer force field (SQMOFF) method to model helical and planar poly(*p*-phenylene) (PPP) and compared the calculated vibrational spectra with experimental data. The 3-21G basis set was found to accurately reproduce vibrational frequencies of benzene and biphenyl with a variant of Pulay's scaling method. This scaling procedure used only 10 scaling factors. The optimized values of the scaling factors were in the 0.6912–0.8725 range as determined from benzene and biphenyl and were taken as fixed parameters in the polymer calculation. The results were a significant improvement over previously calculated frequencies, indicative of excellent transferability of scaling factors from benzene and biphenyl to the polymer. No significant difference was found between the IR spectra of helical and planar PPP. However, a better overall agreement for the Raman spectra was found with nearly planar PPP. Further evidence supporting the nearly planar model comes from the Raman intensity ratio of the 1280 to 1220 cm^{-1} peaks (I_{1280}/I_{1220}) in PPP. Therefore, we concluded that the most probable structure of PPP is nearly planar. All earlier assignments of normal modes by Furukawa based on calculations by Zannonni and Zerbi, Božović and Raković, and Krichene et al. were confirmed except for two bands. Limitations of Zerbi's Я mode model were discussed with respect to Raman intensity predictions.

I. Introduction

To many polymer chemists and material scientists, poly(*p*-phenylene) (PPP) is an attractive and interesting polymer because of its exceptional chemical and thermal properties. This polymer not only is thermally stable up to 450 °C in air but rigid-rod-like PPP also possesses high mechanical strength.[1] However, to the chagrin of polymer technologists, step-growth polymerized PPP is insoluble and not melt processible. The insolubility of PPP presents a problem in the step-growth route to PPP because only short chains are obtained.[1b] Thus, in order to obtain higher molecular weight PPP, an alternative method using the precursor route reported by Gin et al.[2] has attracted much interest. However, the problem of processibility still poses a major hinderance for PPP to become viable for practical applications.

Slightly more than a decade ago, PPP emerged at the forefront of polymer research when it was found to be conductive upon doping with AsF_5.[3] With this discovery came a revival of interest in PPP, and this escalated a series of intensive studies on its structure and electronic properties. Although these studies successfully mapped out the structures of *p*-phenylene oligomers[4-6] and produced some X-ray crystallographic data on the polymer, there was no direct experimental data to conclude unambiguously whether the PPP chain was planar or not. The conclusion was, inferring from oligomer structures, that PPP was likely nonplanar with an inter-ring torsion angle of about 23°.[7] On the other hand, no theoretical work was done to address this structural question, although in the late 1980s Zannonni and Zerbi[8] and Lefrant et al.[9-11] independently calculated the normal-mode frequencies and made assignments of observed IR and Raman bands. These calculations are based on a dynamical force field method whose initial force constants are empirical. The success of this method relies heavily on sound estimates of numerous force constants. Furthermore, the geometries of the polymer have to be known or assumed. In their studies, both groups further assumed a planar structure for PPP. Although the emphases of their studies differed, the common feature of their reports was the assignments of observed IR and Raman bands available at that time. While the two groups arrived at qualitatively similar vibrational frequencies at $k = 0$ (the only allowed k-point for a planar structure), they disagreed by as much as 60–70 cm^{-1} for some of the frequencies. Both also noted the inability of their models to reproduce accurately the frequency of the A_g mode observed at 1220 cm^{-1}. Their results and ours will be compared, with experiment and each other, later on in this paper. There also exists a rather unique feature of PPP Raman spectra concerning the intensity ratio of the 1280- and 1220-cm^{-1} peaks which was not explored in these earlier theoretical studies. It was Lefrant et al.[9] who observed experimentally that the intensity ratio I_{1280}/I_{1220} decreases with PPP chain length. This observation may be explained with the fact that, the 1220-cm^{-1} mode being characteristic of a para-substituted benzene, its intensity increases as the number of such substituted units increases.

The study on vibrational spectra of PPP has been mainly limited by the paucity of the number of peaks observed experimentally. Nonetheless, with the recent efforts by Furukawa et al. a PPP Raman spectrum which shows four additional very weak peaks was reported.[12] It is conceivable that this added information will aid in our attempt to address the following three issues: (1) calculation of the phonon dispersion and vibrational spectra of PPP; (2) relationship between the planarity of PPP and its IR and Raman spectra; (3) theoretical analysis of the intensity ratio I_{1280}/I_{1220} by combining IR and Raman spectroscopic data with accurate theoretical modeling. We build three models, two nonplanar and a planar, using the scaled quantum mechanical oligomer force field (SQMOFF) method developed in this laboratory by Cui and Kertesz.[13] The nonplanar structure is taken to be a helix; the validity of this model for nonplanar PPP will be discussed in section III.D. The SQMOFF method has been successfully tested with linear chain polymers like polyethylene,[13] polyacetylene,[14] and polysilane,[15] a helical sulfur chain,[13] and polymers having rings in the backbones[16] (polythiophene and poly(thienylenevinylene)). With this method we systematically build up both helical and planar PPP from

® Abstract published in *Advance ACS Abstracts*, January 1, 1994.

0024-9297/94/2227-0762$04.50/0

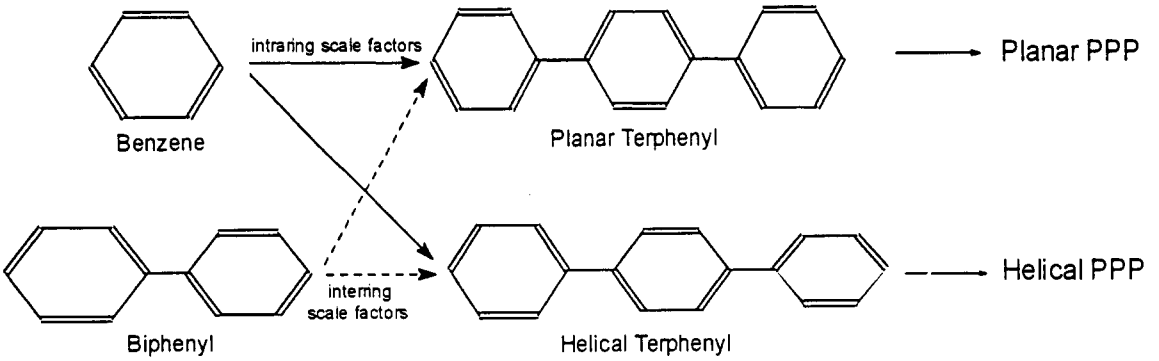

Figure 1. Scheme of the SQMOFF method used in modeling helical and planar PPP. See the text for an explanation.

benzene, biphenyl, and terphenyl and compare these models with experimental data.

II. Methodology

Readers are referred to ref 13 for a detailed description of the SQMOFF method utilized in this study. Nonetheless, for the sake of completeness, we present the following condensed description. The SQMOFF method is based on the k-dependent dynamical matrix $\mathbf{F}(\mathbf{k})$ of the polymer, which can be expressed as[17]

$$\mathbf{F}(\mathbf{k}) = \mathbf{F}(0) + \sum_j \mathbf{F}(j) \exp(i\mathbf{k}ja)$$

where $\mathbf{F}(0)$ is the force matrix of the central unit of an oligomer. Usually a trimer is used, and thus only first-neighbor interactions are included. This force matrix was then used to solve for vibrational frequencies following the Wilsonian **GF** method:

$$\mathbf{F}(\mathbf{k})\,\mathbf{C}(\mathbf{k}) = \mathbf{G}(\mathbf{k})\,\omega(\mathbf{k})\,\mathbf{C}(\mathbf{k})$$

where $\mathbf{G}$ is a diagonal matrix whose elements are the reciprocal atomic masses of the unit cell and $\mathbf{F}$ is expressed in Cartesian coordinates. The eigenvalues $\omega_j(\mathbf{k})$ are $4\pi^2\nu_j(\mathbf{k})^2c^2$, where $\nu_j(\mathbf{k})$ are the vibrational frequencies of the jth phonon branch, c is the speed of light, and $\mathbf{k}$ is a reciprocal lattice vector in the first Brillouin zone. The $\mathbf{C}(\mathbf{k})$ eigenvectors describe the normal modes. The IR intensities and Raman scattering activities were obtained from the dipole moment and polarizability derivatives taken with respect to Cartesian coordinates of the central unit of the trimer.

We used Gaussian 90[18] and Gaussian 92[19] *ab initio* programs to perform geometry optimizations, force constant calculations, and dipole moment/polarizability derivatives, with the basis set being the double-ζ quality 3-21G. As will be shown by our results on benzene and biphenyl, this basis set was a justifiable compromise between cost and accuracy. Because the *ab initio* SCF method systematically overestimates force constants, it was necessary to incorporate a set of empirical scaling factors[20,21] determined by least-squares fitting to the observed frequencies of the monomer and dimer. It must be emphasized that scaling factors were introduced to correct for systematic errors incurred at the SCF level. No other parameters were used in the calculations, and no spectral data of the polymer were used in the scaling process.

Our use of benzene, biphenyl, and terphenyl (planar and twisted) for modeling PPP is summarized in Figure 1.

First, we optimized the geometries of these molecules with appropriate symmetry restrictions, *i.e.*, D_{2h} and D_2 symmetries for benzene and biphenyl, respectively. Next, we scaled the force constants of benzene obtained at the 3-21G level using a variant of Pulay's scaling scheme:[20]

$$F'_{i,j} = (S_iS_j)^{1/2}F_{i,j} \qquad (1)$$

where $F'_{i,j}$ is the scaled force constant, $F_{i,j}$ is the unscaled 3-21G level calculated force constant, and S_i and S_j are the scaling factors for internal coordinates i and j, respectively. The modification made here is the inclusion of one additional scaling factor for CC/CC coupling. This modification is necessary, as pointed out by Pulay et al., due to a significant correlation effect.[21] Even though eq 1 reduces the off-diagonal force matrix elements, it still tends to overestimate the CC/CC coupling constants of benzene.[21] Incidentally, the opposite has been observed for CC/C=C and C=C/C=C coupling in butadiene.[22] These force constants are greatly underestimated at the SCF level, and hence eq 1 is inadequate; *i.e.*, it tends to underestimate these coupling constants in butadiene. It is apparent from these observations that, in systems where correlation effects are significant, the use of an appropriate scaling factor for CC/CC coupling constants is vital in obtaining a good fit.

The definitions of all internal coordinates used are described in Table 1 and Figure 2. While scaling involves the use of internal coordinates, the Wilsonian **GF** method and Gaussian programs utilize Cartesian coordinates; hence, transformation between internal and Cartesian coordinates is necessary.

Next, the optimized scaling factors from benzene were used as initial scaling factors in the least-squares refine-

Table 1. Unnormalized Internal Coordinates of Benzene,[a] Biphenyl,[b] and Terphenyl[c]

no.	internal coordinates[d]	description (see Figure 1)
	Intraring	
1	$R_1, \ldots, R_m$	C–C stretch
2	$r_1, \ldots, r_n$	C–H stretch
3	$\gamma_1, \ldots, \gamma_n$	C–H wag
4	$(\varphi_1 - \varphi_1'), \ldots, (\varphi_n - \varphi_n')$	C–H in-plane deformn
5	$(\alpha_1 - \alpha_2 + \alpha_3 - \alpha_4 + \alpha_5 - \alpha_6)$ $(2\alpha_1 - \alpha_2 - \alpha_3 + 2\alpha_4 - \alpha_5 - \alpha_6)$ $(\alpha_2 - \alpha_3 + \alpha_5 - \alpha_6)$	ring deformn
6	$(\tau_1 - \tau_2 + \tau_3 - \tau_4 + \tau_5 - \tau_6)$ $(-\tau_1 + 2\tau_2 - \tau_3 - \tau_4 + 2\tau_5 - \tau_6)$ $(\tau_1 - \tau_3 + \tau_4 - \tau_6)$	ring torsion
	Inter-ring	
7	RR	C–C stretch
8	$\Lambda_1, \ldots, \Lambda_p$	C–C wag
9	$\phi_1, \ldots, \phi_p$	C–C in-plane deformn
10	δ	inter-ring torsion

[a] Benzene: $m = 6$, $n = 6$. [b] Biphenyl: $m = 12$, $n = 10$, $p = 2$. [c] Terphenyl: $m = 18$, $n = 14$, $p = 4$. [d] γ_1 is the angle between the C–H_1 bond and the $C_1C_2C_6$ plane, etc. τ_1 is the torsion angle $C_6C_1C_2C_3$, and so on. δ is a linear combination of all the torsion angles along the inter-ring C–C bond, etc.

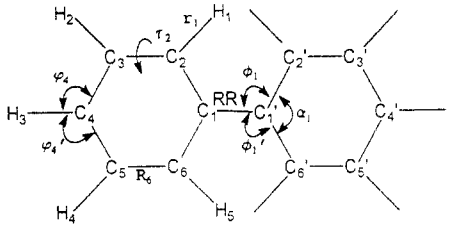

Figure 2. Descriptions of internal coordinates used in this study. See also Table 1.

Table 2. Calculated and Experimental Frequencies (cm^{-1}) of Benzene

symmetry	exptl[a]	this work	ref 20
	In-Plane		
A_{1g}	3073	3083	3095
	993	992	983
A_{2g}	1350	1352	1365
B_{1u}	3057	3044	3051
	1010	1010	997
B_{2u}	1309	1307	1297
	1146	1159	1162
E_{2g}	3056	3053	3061
	1599	1605	1607
	1178	1177	1183
	606	605	607
E_{1u}	3064	3069	3080
	1482	1474	1482
	1037	1034	1036
	Out-of-Plane		
A_{2u}	673	663	667
B_{2g}	990	990	996
	707	706	701
E_{1g}	846	841	843
E_{2u}	967	974	969
	398	401	402
error[b]		6.0	8.3

[a] Compiled by Pulay et al.[20] [b] Defined as $[\sum_i (x_i - y_i)^2/(N-1)]^{1/2}$ where x_i and y_i are experimental and calculated frequencies, respectively; N is the number of normal modes.

ment of scaling factors for biphenyl including a separate scaling factor for CC/CC coupling. Finally, we transferred all scaling factors of benzene, together with the inter-ring in-plane and out-of-plane bend and torsion scaling factors of biphenyl to scale the force constants of terphenyl. As described earlier, we extracted the central block and the first-neighbor interaction block of this scaled force matrix for the subsequent polymer calculations.

We chose terphenyl and not the more desirable larger oligomer, *e.g.*, pentaphenyl, primarily due to limited computational resources. However, we were convinced from our earlier experience with polythiophene and poly(thienylenevinylene)[16] that the use of a trimer is sufficient, because of the fast convergence of the harmonic force field with respect to the number of neighbors.

III. Results and Discussion

A. Benzene, Biphenyl, and Terphenyl. One advantage of the SQMOFF method is the use of smaller molecules at the early stage of the calculations. By analyzing the results of smaller molecules, we are able to examine the suitability of the 3-21G basis set used. In Table 2, we see an excellent agreement between the scaled calculated and experimental frequencies of benzene. The root-mean-square error of only 6.0 cm^{-1} affirms the suitability of the 3-21G basis set with the use of modified Pulay's scaling scheme.[21]

By imposing a D_2 symmetry and using the 3-21G basis set, we obtained an optimized geometry of biphenyl, shown in Figure 3. The geometry of biphenyl is dependent on

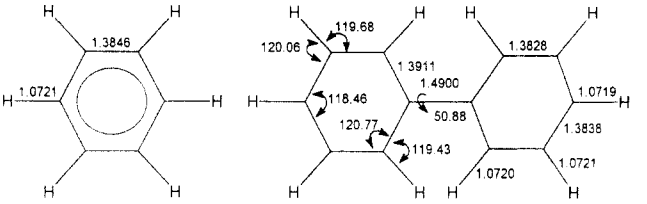

Figure 3. Left: Optimized geometry of benzene. Right: Optimized geometry of biphenyl. The units for bond length and angle are angstroms and degrees, respectively.

the state of aggregation and is characterized by the inter-ring torsional angle. Solid biphenyl was found to be planar by X-ray crystallography.[23,24] In the gaseous state, this torsional angle was determined to be 44.4° ± 1.2° by gas electron diffraction (GED).[25] In the molten phase, biphenyl has an intermediate torsional angle of about 18°.[26] The inter-ring bond length of biphenyl was found to be 1.505 Å by GED and 1.493 Å by X-ray diffraction, indicating a slight dependence on planarity. Within the limit of SCF calculations, our calculated geometry shows a reasonably good agreement with these experimental values.

Table 3 lists our calculated frequencies for biphenyl. These results were obtained using the same procedure described for benzene; the inter-ring internal coordinates are nos. 7–10 in Table 1. These calculated frequencies compare favorably with experimental data obtained with gaseous biphenyl, as well as theoretical values from previous reports.[27,28] Because of the large number of vibrational frequencies involved, we consider the root-mean-square error of 10.2 cm^{-1} to be reasonably good. This result is also consistent with the observation on benzene that the 3-21G basis set is sufficient for our purposes.

The calculated geometries of terphenyl are shown in Figure 4, which form the basis of the polymeric PP calculations.

B. Helical and Planar PPP. Before we analyze our results, a review of the selection rules for helical and planar PPP is helpful. In the case of planar PPP, its factor group is isomorphous with the point group D_{2h}. Thus, the selection rules for planar PPP are such that IR and Raman activities are mutually exclusive, and all *gerade* modes are Raman active while all *ungerade* modes are IR active. The irreducible representations of planar PPP have been worked out by Zannonni and Zerbi.[8] Suffice it to say that its factor group is isomorphous with the D_{2h} point group at the center and the edge of the Brillouin zone. Therefore, it works out that, at $k = 0$, there are 14 Raman-active modes, 10 IR-active modes, and 2 spectroscopically inactive modes: $5A_g + 1B_{1g} + 3B_{2g} + 5B_{3g} + 2A_u + 4B_{1u} + 4B_{2u} + 2B_{1u}$.

The selection rules of helical PPP are different from those of planar PPP. Theoretically, all frequencies at $k = 0$, $k = \theta/h$, and $k = 2\theta/h$ are Raman active (h is the translation per repeat unit, and θ is the angle of rotation of the screw).[13] In addition, frequencies at $k = 0$ and $k = \theta/h$ are IR active. Based on this rule, it appears that the PPP spectrum should be more complex if its structure were helical. However, intensity plays a major role as well. Therefore, the relatively simple nature of PPP spectra may be a consequence of weak intensities of many allowed modes. From our calculations, we found four intense Raman frequencies and four strong IR frequencies in the 700–1600-cm^{-1} region, most of which have flat phonon branches (see Figure 5). To make matters less complex, it seems prudent that, for ease of description and comparison with other previously published results, we ought to label our calculated frequencies with D_{2h} representation.

Table 3. Calculated and Experimental Frequencies of Biphenyl

symmetry	exptl[a] (gas, D_2)	this work (D_2)	ref 27 (D_{2h})	ref 28 (D_2)
A_g	1613	1620	1628	1690
	1505	1516	1497	1527
	1282	1282	1285	1338
	1190	1190	1175	1192
	1029	1016	1030	1024
	1003	994	989	998
	740	740	758	745
	315	305	279	272
B_{1g}	964	974	963	963
	838	831	833	833
	403	397	409	409
B_{2g}	979	986		987
	917	925		909
	778	774		755
	670	684		694
	543	538		515
	269	274		239
B_{3g}	1595	1585	1610	1609
	1455	1462	1482	1449
	1376[b]	1346	1367	1337
	1317	1310	1299	1292
	1158	1171	1167	1155
	1090[b]	1079	1071	1069
	615	617	599	607
	367	350	392	342
A_u	964	969		963
	838	832		833
	403	405		409
	55[c]	60		
B_{1u}	1595	1595	1607	1610
	1481	1480	1480	1483
	1174	1187	1178	1193
	1042	1033	1039	1040
	1007	1003	1005	1020
	990	992	983	992
	609	614	625	611
B_{2u}	1567	1566	1567	1608
	1430	1434	1439	1430
	1337	1333	1363	1326
	1266	1261	1270	1295
	1155	1171	1168	1161
	1072	1068	1054	1055
	628[b]	629	610	622
	112	117	119	96
B_{3u}	964	968		987
	902	906		898
	902	906		726
	735	738		703
	486	517		431
		117		91
error		10.2	13.3	21.3

[a] From ref 28. [b] From ref 27. [c] From ref 34.

We emphasize that these labels are not the true symmetry of a helical PPP chain but the local symmetry of a repeat unit, and they are adopted for convenience only. The frequencies and intensities at $k = 0$ are also listed in Table 4 for comparison purposes. All other frequencies not listed can be obtained from the phonon branches shown in Figure 5.

The scaling factors used in our calculations together with some selected average scaled force constants are listed in Table 5. These force constants which are similar to those obtained by Buisson et al.[10] explain the overall similarity of the two calculations. Because of the planar structure imposed on terphenyl, the derivative calculations were performed at a saddle point. Consequently, we obtained a negative force constant for inter-ring torsion. Furthermore, due to rounding errors, we obtained imaginary frequencies for parts of the transverse acoustic branch of helical PPP which was omitted from Figure 5. (See also refs 13, 15, and 22 for discussions on obtaining imaginary frequencies.) Fortunately, there is practically no coupling between these low-frequency modes and the prominent peaks observed experimentally in the 700–1600-cm^{-1} region.

First of all, we make an observation on the dependence of vibrational frequencies on the conformation of PPP. Comparing the out-of-plane vibrational frequencies of planar and helical PPP (Table 4), we found that, with the exception of a low-lying B_{3u} mode, there is an upward shift toward higher frequencies in going from planar to helical conformation. Similar, but much smaller shifts, were also reported for 5-membered ring systems, namely, for polythiophene[29] and polypyrrole.[30] However, no such straightforward trend is observed for the in-plane modes.

Next, we compare our calculated results with previous calculations and experimental spectra. Table 4 lists our calculated results alongside experimental data; calculated results are reported by Zannonni and Zerbi[8] and by Buisson et al.[10] The latter reported only the in-plane frequencies. In general, our results are in better agreement with those reported by Buisson et al.[10] While we overestimated the first A_g mode, the first B_{3g} mode frequency calculated by Buisson et al. is much higher than ours. To summarize, only Buisson et al. calculated the first A_g mode to be lower in frequency than the first B_{3g} mode. Unfortunately, no experimental data are available to verify the frequency of the B_{3g} mode. Compared with experimental data, our helical (20°) model has the best agreement. The most notable feature of our results is that, for the first time, the 1220-cm^{-1} mode is reproduced in the calculation. This frequency was not reproduced by previous investigators, and in our helical (50°) PPP model it occurs at too low frequency. While the reason for the inability of our helical (50°) PPP to reproduce this frequency may be a structural one, the inability of the planar PPP used by earlier investigators may originate from the empirical force fields used. As stated earlier, our force constants are similar to those used by Buisson et al.; the major differences come from the coupling force constants. On the basis of this comparison with experimental frequencies above, we conclude that our helical (20°) model more accurately represents the structure and the force field of PPP.

In order to make a more in-depth comparison between our results and experiment, we simulated IR and Raman spectra with our calculated frequencies and intensities. We generated each peak using a Gaussian function:

$$I_j = I_i \exp(\nu_j^2/2\sigma)$$

where I_i = calculated intensity of the ith mode, ν_j is the frequency relative to the ith normal-mode frequency, and $\sigma = 25$ cm^{-1}.

The IR spectrum reported by Shacklette et al.[7] is reproduced in Figure 6. By comparing this spectrum with those calculated for helical (50°) and planar PPP, we found equally good agreement between the calculated spectra and the measured IR spectrum, not allowing us to differentiate between the two models (helical vs planar).

We conducted a similar comparison between the calculated Raman spectra and the latest Raman spectrum of PPP obtained by Furukawa et al.,[12] as depicted in Figure 7. In this spectrum, a number of weak bands not previously observed are present, presumably because the excitation laser energy was set at 1064 nm which is off-resonance. At first glance, both calculated spectra appeared to show a good resemblance to the experimental spectrum. However, on closer inspection, two unique features of each calculated spectrum are apparent: the frequency near 1220 cm^{-1} and

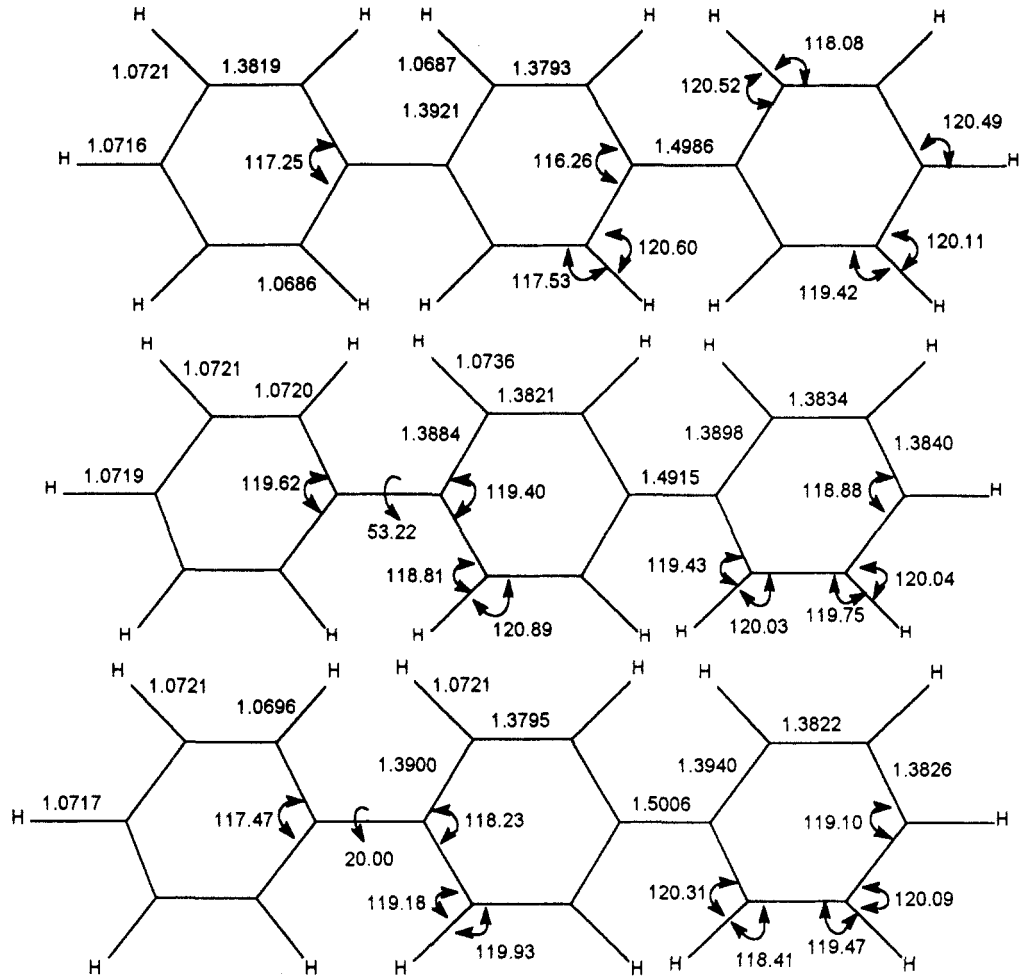

Figure 4. Optimized geometry of terphenyls. Top: Planar model used to model planar PPP. Middle: Twisted terphenyl, geometry fully optimized, used to model helical PPP. Bottom: Twisted terphenyl, geometry optimized with a fixed inter-ring torsion angle of 20°, used to model helical PPP. The units for bond length and angle are angstroms and degrees, respectively.

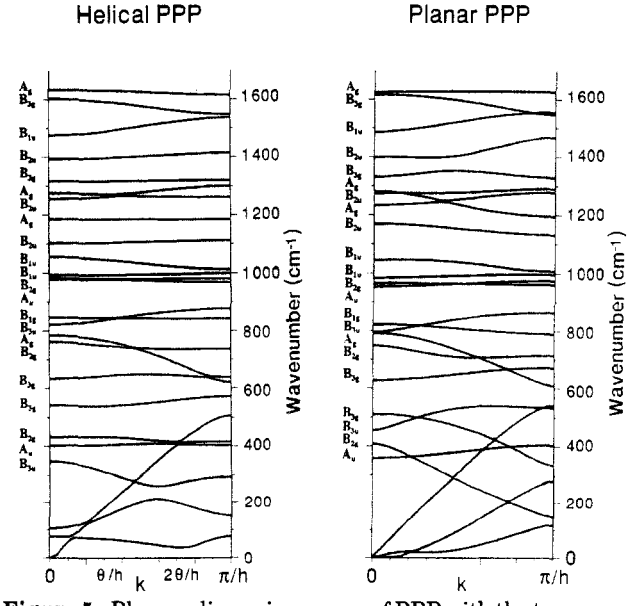

Figure 5. Phonon dispersion curves of PPP with the transverse acoustic branch and flat branches of C–H stretches omitted. Left: Helical (50°) PPP (C–H stretch frequencies at $k = 0$ are 3039, 3042, 3059, and 3060 cm^{-1}). Right: Planar PPP (C–H stretch frequencies are 3073, 3073, 3117, and 3122 cm^{-1}).

the intensity. Regarding frequency, we found a larger deviation of 37 cm^{-1} from the observed 1223-cm^{-1} peak for helical (50°) PPP as compared to a deviation of 10 cm^{-1} of planar PPP. Besides the underestimation of this mode, an overestimation of the 1595 cm^{-1} by 40 cm^{-1} was also observed for the helical (50°) model. On the basis of the errors obtained for benzene and biphenyl, we may conclude that this deviation (~40 cm^{-1}) is too large. Furthermore, it must be noted that the inter-ring stretching mode (1280 cm^{-1}) was accurately reproduced. Since these three modes are coupled to each other, any attempt to narrow the deviation of one mode by changing its scaling factor will inevitably increase the deviations of the other modes; therefore, it is obvious that the force field cannot be improved significantly by varying scaling factors. The other notable difference between these two calculated spectra was found in the relative intensity of the 1280- and 1220-cm^{-1} peaks, which are of opposite trends. Lefrant et al.[11] showed through a series of experiments using *p*-phenylene oligomers and PPP having different chain lengths that the intensities of these two peaks were dependent on the number of phenyl rings, provided the excitation energy remained constant. They found that, as the number of phenyl rings increases, the intensity of the 1280-cm^{-1} band decreases and that of 1220 cm^{-1} increases. Using experimental data of Krichene et al.,[31] we obtained a straight plot of $\ln(I_{1280}/I_{1220})$ vs $1/N$ (where N is the number of phenyl rings) in Figure 8 and extrapolated this straight line to obtain the limiting intensity ratio of 0.18 for an infinite chain. Our calculated intensity ratios are 0.06, 0.33, and 6.8 for planar, helical (20°) and helical (50°) PPP, respectively. Thus, it is apparent that this phenomenon was reproduced very well by the planar and helical (20°) PPP but not at all by the helical (50°) PPP model.

Table 4. Calculated and Experimental Frequencies (cm^{-1}) and Intensities[a] of PPP

	calcd[b]									
	this work (planar)		helical 20°		helical 50°		ref 8	ref 10	exptl	
symmetry	freq	intensity	freq	intensity	freq	intensity	(planar) freq	(planar) freq	freq	ref
					In-Plane Modes					
Raman active										
A_g	1626	1900	1630	1343	1635	400	1661	1601	1595 (vs), 1593 (vs)	11, 12
	1282	43	1270	122	1277	120	1289	1290	1280 (w), 1281 (m)	11, 12
	1233	670	1222	374	1186	17	1127	1184	1220 (m), 1223 (m)	11, 12
	792	11	785	11	786	24	846	802	805 (vw), 796 (vw)	11, 12
B_{3g}	1601	2.8	1623	45	1603	0.37	1654	1652		
	1325	2.2	1361	1.6	1317	2.3	1328	1343		
	625	6.5	645	5.8	634	6.0	602	616	623 (vw)	12
	488	0.03	509	0.16	542	0.22	460	418		
IR active										
B_{1u}	1487	69	1486	60	1477	42	1510	1490	1482 (s)[c]	7
	1045	0.02	1053	0.09	1057	0.05	1051	1044		
	984	4.1	990	3.6	994	10	968	1004	998 (m)	7
B_{2u}	1399	8.1	1400	9.3	1395	8.3	1440	1412	1400 (m)	7
	1275	2.6	1244	1.0	1256	0.72	1268	1343		
	1162	1.2	1109	5.9	1104	5.0	1075	1118		
					Out-of-Plane Modes					
Raman active										
B_{1g}	823	3.6	821	3.0	847	3.4	834			
B_{2g}	968	21	981	6.7	984	4.2	945		999 (vw)	12
	754	9.5	758	7.3	763	2.9	760			
	410	7.4	432	5.0	432	4.6	402		409 (w)	12
IR active										
B_{3u}	797	86	809	80	823	62	790		804 (s)	7
	457	12	409	1.2	349	1.0	458			
nonactive										
A_u	951	0.00	976	0.04	979	0.33	961			
	367	0.00	403	0.6	403	0.02	401			

[a] IR intensities in km/mol; Raman scattering activity in Å⁴/amu. [b] Refer to Figure 4 for CH frequencies. [c] Also occurs at 1485 cm^{-1} in the Raman spectrum (see text).

Table 5. Force Constants and Scale Factors of PPP[a]

		force constants	
description	scaling factors	helical (50°)	planar
C–C stretch	0.8725	6.653	6.610
C–C inter-ring stretch	0.8725	4.505	4.573
C–H stretch	0.8279	5.103	5.268
C–H in-plane deformn	0.7666	0.506	0.535
C–C in-plane deformn	0.9550[b]	1.001	1.647
C–H wag	0.7134	0.443	0.399
C–C inter-ring wag	0.7848[b]	0.525	0.558
ring deformn	0.7438	1.221	1.255
		1.200	1.182
		1.269	1.420
ring torsion	0.7367	0.283	0.230
		0.363	0.312
		0.314	0.282
inter-ring torsion	0.9904	0.025	−0.041[c]
CC/CC coupling	0.6912		

[a] The units are mdyn/Å for stretching and mdyn·Å/rad² for angle. [b] Transferred from biphenyl; all others are from benzene. [c] See text for an explanation.

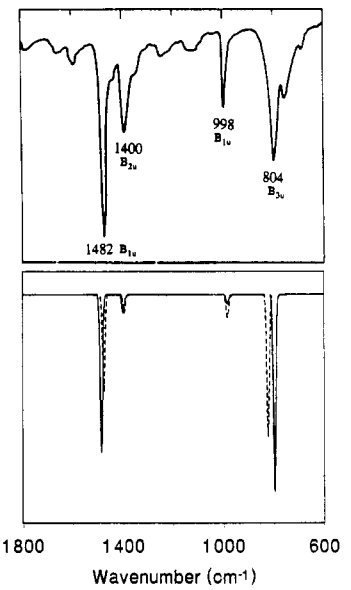

Figure 6. Top: IR spectrum of PPP by Shacklette et al. Assignments are as indicated; see also Table 5. Bottom: Calculated spectra ((—) planar PPP; (· · ·) helical). Top part: Reprinted with permission from ref 7. Copyright 1979 Elsevier Sequoia S.A.

After analyzing the overall features of our calculated spectra, we proceeded with assignments of both IR and Raman bands, listed in Table 4. Except for two modes, we are in agreement with assignments made by Furukawa based on normal-mode analyses of Zannonni and Zerbi,[8] Božović and Raković,[32] and Krichene et al.[33] As noted earlier, these investigators based their calculations on the D_{2h} symmetry of PPP, so direct comparison with our planar PPP is straightforward. We differ from Furukawa by assigning the observed 409-cm^{-1} band to be a B_{2g} out-of-plane mode rather than a B_{3g} mode. Furthermore, we disagree with his assignment of the weak 1485-cm^{-1} peak as a B_{3g} (B_{1g} in Furukawa's notation) mode. As shown in Table 4, we found two calculated B_{3g} frequencies in the vicinity of 1485 cm^{-1}. Take the planar PPP for an example; one is 1601 cm^{-1}, and the other is 1325 cm^{-1}, which deviates from the observed frequency by 116 and 160 cm^{-1}, respectively. We therefore considered this assignment unjustifiable because of such great deviations. Rather, it is possible that this observed weak Raman band of 1485 cm^{-1} is the IR-active B_{1u} mode, which manifests itself as a weak Raman band due to structural disorder. The good agreement between experimental and calculated isotropic shifts as shown in Table 6 further supports our assignments.

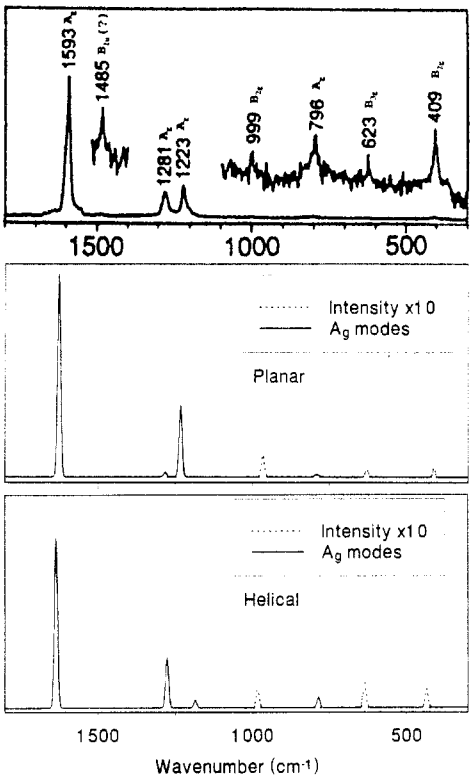

Figure 7. Top: Resonance Raman spectrum of PPP (λ_{exc} = 1064 nm) by Furukawa et al., reproduced from ref 12 with permission. Assignments are as indicated; see also Table 5. Middle: Calculated Raman spectrum of planar PPP. Bottom: Calculated spectrum of helical (50°) PPP.

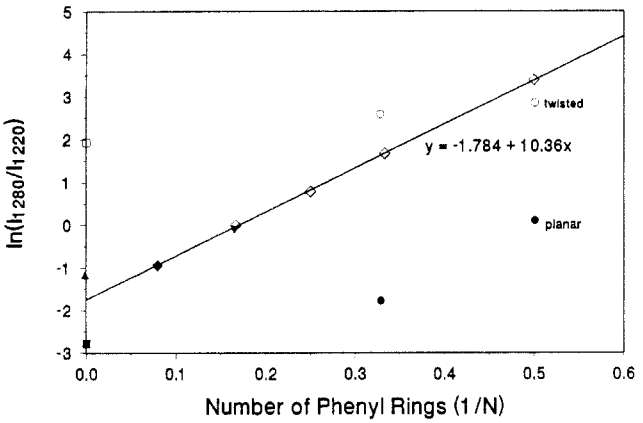

Figure 8. Plot of experimental (on films) and calculated Raman intensity ratios of the 1280- and 1220-cm^{-1} modes vs reciprocal of the number of phenyl rings: (◇) experimental values of oligomers, λ_{exc} = 647.1 nm (30, 5.3, 2.2, 0.96; see ref 31); (◆) PPP polymerized by Fauvarque's electrochemical method (0.34, N is chosen such that this point falls on the fitted line; see refs 31 and 35); (▼) Furukawa's PPP polymerized by Yamamoto's method (0.8, estimated from ref 12 and N is chosen such that this point falls on the fitted line); (▲) helical (20°) PPP (0.33, calculated); (□) helical (50°) PPP (6.8, calculated); (■) planar PPP (0.06, calculated); (●) planar biphenyl and terphenyl) (1.2, 0.17, calculated); (○) 50° twisted biphenyl and terphenyl (16, 14, calculated). Values in parentheses are intensity ratios.

Finally, for completeness, we showed in Figure 9 the atomic displacements of all A_g modes and assigned IR modes.

C. The ℜ Mode and Raman Intensity. There are three current models in circulation, which attempt to explain the resonance Raman effect in polyconjugated polymers. The first is the conjugation length (CL) model[36] which utilizes Albrecht's theory and emphasizes that in real samples there is a conjugation length distribution strongly affecting the observed spectrum. The second is the amplitude mode (AM) model which is a solid-state approximation[37] and treats the electron–phonon coupling as an empirical parameter. Last, there is the effective conjugation coordinate (ECC) model which attempts to explain the results of the AM model with molecular dynamics[38] and an $F_{\mathfrak{R}}$ parameter which represents an empirical force constant for a particular mode, the ℜ mode. It is not the intention of this paper to compare these three models, which has been done in great detail by others. For instance, Kürti and Kuzmany[36] have shown the similarities of these three models for the case of polyenes. In addition, Schaffer et al.[39] have also discussed the AM and ECC models with reference to a series of spectral results obtained from oligomers of polyenes. The ECC model is easily extended to ring systems. Because PPP is a polymer having rings in the backbone and since the ECC mode also uses the Wilsonian **GF** method (as in our polymer calculations), we can compare this model with our calculations for the infinite poly(*p*-phenylene). As required by the ECC model, and it will become apparent later, we use only our planar PPP model for this comparison.

Zerbi et al.,[38] in describing the ECC model, state that there exists a certain $\mathfrak{R}_1$ mode which is "a totally symmetric linear combination of internal coordinates which describes the variation of the equilibrium geometry Δx^{eg} from the ground state g to the first excited state e". Except for the perfect one-dimensional polymers, $\mathfrak{R}_1$ is not a normal mode. However, if the $\mathfrak{R}_1$ mode is coupled to some normal modes, it lends intensity to these normal modes. In the case of the Raman spectrum, these normal modes are the A_g modes. In other words, there exists an intensity dependency of A_g modes on the $\mathfrak{R}_1$ mode, which is considered to be the mode which most strongly couples the geometry to the electronic structure. According to the ECC model, the intensity of the kth mode is proportional to the square of its eigenvector, *i.e.*, $I_k \propto |L_{\mathfrak{R}k}|^2$, where $L_{\mathfrak{R}k}$, as we shall see later, is simply the scalar product of the kth normal mode and the $\mathfrak{R}_1$ mode. Accordingly, it can be said that the intensity ratio of two A_g modes may be written as $I_j/I_k = |L_{\mathfrak{R}j}|^2/|L_{\mathfrak{R}k}|^2$. Let $\mathfrak{R} = \mathbf{Vx}$ and $\mathbf{Q} = \mathbf{L}_{\mathfrak{R}}\mathfrak{R} = \mathbf{Cx}$, where $\mathbf{V}$ and $\mathbf{L}_{\mathfrak{R}}$ are transformation matrices, $\mathbf{x}$ is the Cartesian displacement vector, and $\mathbf{Q}$ is the normal mode in Cartesian coordinates. Therefore,

$$\mathbf{L}_{\mathfrak{R}} = \mathbf{V}^{-1}\mathbf{C} \tag{2}$$

We have obtained $\mathbf{C}$ from our polymer calculations using the Wilsonian **GF** method, and now we need only to find $\mathbf{V}^{-1}$. However, since we are only interested in the $\mathfrak{R}_1$ mode, only this mode needs to be defined and transformed to the Cartesian displacement vector. We set up the $\mathfrak{R}_1$ internal coordinate (Figure 10) defined as:[38]

$$\mathfrak{R}_1 = N(2\delta r_2 - \delta r_1 - \delta r_3)$$

where N is the normalization factor. The numerical values of $L_{\mathfrak{R}k}$'s can thus be calculated from eq 2. With respect to the smallest value, we obtain the relative intensities of the four A_g modes in the descending frequency as 19.5, 1.19, 1.21, and 1. In other words, the $\mathfrak{R}_1$ mode predicts correctly one very intense peak for the highest frequency A_g mode. Our detailed calculations show that only A_g modes have any appreciable intensity, in agreement with the ECC model. The relative intensities of the three weaker modes do not agree, however, with experiment. For instance, the I_{1280}/I_{1220} ratio is 1.19/1.21 ≈ 1.0. This value is about 5 times greater than the value estimated from experimental data (0.18) as discussed above, around Figure 8. This leads to the conclusion that the ECC model

Table 6. Calculated and Experimental Frequencies of Hydrogenated and Deuterated PPP (cm^{-1})

	exptl[a]			calcd (planar)			helical (20°)			helical (50°)		
	$(C_6H_4)_x$	$(C_6D_4)_x$	shift	$(C_6H_4)_x$	$(C_6D_4)_x$	shift	$(C_6H_4)_x$	$(C_6D_4)_x$	shift	$(C_6H_4)_x$	$(C_6D_4)_x$	shift
Raman												
A_g	1595	1568	27	1626	1598	28	1630	1601	29	1635	1609	26
	1280	1262	18	1282	1241	41	1270	1239	31	1277	1257	20
	1220	894	326	1233	909	324	1222	898	324	871	871	315
	805			792	768	24	785	759	26	750	750	36
IR												
B_{1u}	1482	1355	127	1487	1357	130	1486	353	133	1477	1352	125
		977		1045	983	62	1053	986	67	1057	990	67
	998	816	182	984	815	169	990	824	166	994	822	172
B_{2u}	1400	1329	71	1399	1334	65	1400	1315	85	1395	1310	85
B_{3u}	804			798	786	12	809	796	13	823	798	25

[a] From ref 10.

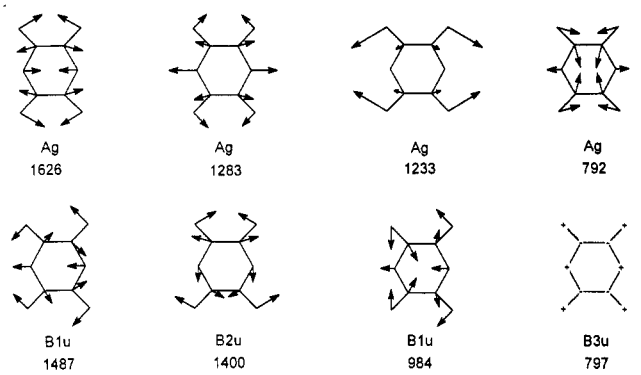

Figure 9. Atomic displacements of major Raman-active modes (top) and IR-active modes (bottom) of planar PPP.

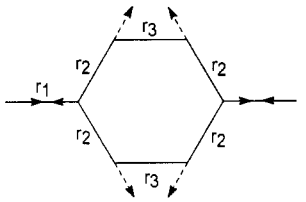

Figure 10. Internal coordinates of the $\mathfrak{R}_1$ mode.

proposed by Zerbi may be oversimplified for PPP. However, to definitively determine the applicability of the $\mathfrak{R}_1$ mode hypothesis to conjugated polymeric systems, a broader study using more polymers is necessary.

D. Conformations of Nonplanar PPP. Our discussion on the intensity ratio has so far centered around planar PPP; we now move to the question on the effect of conformation. The effect of conformation on the IR and Raman spectra of polymers is beginning to be recognized as a topic of significance in extracting conformational information.[29,40,41] In this work, we have studied the dependence of intensity on the conformation of PPP using planar and helical models since we are unable to model a truly random chain with sufficient accuracy. Consequently, we cannot preclude the possibility that PPP may be a random chain because of the lack of theoretical data. In an attempt to gain insight into the dependence of intensity on conformation, we turn to the terphenyl molecule. In Table 7, we list four selected unscaled frequencies and intensities of three terphenyl conformers calculated with the Gaussian 92[19] program. These four bands are selected based on their high intensities. The three terphenyl conformers chosen are planar, G^+G^+, and G^+G^-, the last two are illustrated in Figure 11. No significant difference in the frequencies and intensities of the two different twisted conformers is observed. Rather, consistent with the results of PPP, the planar terphenyl has frequencies and intensities quite different from those of the twisted terphenyls. We may conclude from the

Table 7. Unscaled Frequencies and Intensities of Three Terphenyl Conformers[a]

	planar		G^+G^+		G^+G^-	
mode[b]	frequency	intensity	frequency	intensity	frequency	intensity
A_g	1783	1109	1783	541	1783	540
A_g	1773	1718	1773	114	1773	111
A_g	1398	220	1385	241	1385	234
A_g	1350	1272	1333	17	1333	17

[a] Units for frequency and intensity are cm^{-1} and $Å^4$/amu, respectively. G^+G^+ and G^+G^- refer to nonplanar conformations, as illustrated in Figure 11. [b] With reference to planar terphenyl.

Figure 11. Left: Terphenyl (G^+G^+) used to model helical PPP. Right: Terphenyl (G^+G^-). (—) 1st ring, (—) 2nd ring, (|||||) 3rd ring.

above observations that nonplanar terphenyl, whether helical or random, may not be differentiated from each other but may be differentiated from the planar one using vibrational spectroscopy.

As stated earlier, we are not able to model randomly twisted PPP and totally eliminate the possibility of PPP having this structure; nonetheless, we see no evidence that vibrational modes of randomly twisted PPP should resemble those of planar PPP.

IV. Conclusion

We have applied the SQMOFF method to model helical and planar PPP using a modest 3-21G basis set. This method allowed us to compare calculated vibrational frequencies of these models to those obtained experimentally and theoretical calculations carried out earlier with the dynamical force field method. We obtained a better agreement with experimental data with the SQMOFF method as compared to those calculated with the dynamical force field method. In addition, for the first time the 1220-cm^{-1} mode was reproduced accurately by a planar model.

The intensity ratio I_{1280}/I_{1220} of the PPP Raman spectrum was extrapolated to the value of 0.18 for an infinite chain from experimental data, which was used in evaluating the present and earlier calculations. However, this value was calculated to be approximately 1 according to the ECC model, a value which corresponds to sexiphenyl but not to the infinite chain.

We arrived at the conclusion that the structure of the PPP chain was nearly planar (inter-ring torsion angle of less than 20°) based on the following results:

(1) Calculated Raman frequencies of planar and helical (20°) PPP agreed better with those obtained experimentally.

(2) The extrapolated experimental intensity ratio for the infinite chain falls between those of the planar PPP and PPP having an inter-ring torsional angle of 20°. Moreover, the intensity of the 796-cm^{-1} peak is more consistent with the planar and 20° models than with the helical (50°) model.

Finally, we note that the high accuracy achieved with this complex polymeric system using only a small number of scaling factors transferred from smaller molecules is indicative of the reliability of the SQMOFF method. This also demonstrates the significance of the transferability of scaling factors, without which the SQMOFF method will not stand. We are convinced that this method can be used to study the structures of doped polymers as in the case of pristine polymers. The results of doped PPP will be published elsewhere.[42]

Acknowledgment. This work is supported by grants from NSF (DMR-91-15548) and the Pittsburgh Supercomputer Center (DMR920006P). We are grateful to Prof. Serge Lefrant and Dr. C. X. Cui for their insightful discussions.

Supplementary Material Available: Complete force matrix of benzene and complete force matrix and scaling factors of biphenyl (5 pages). Ordering information is given on any current masthead page.

References and Notes

(1) (a) Elsenbaumer, R. L.; Shacklette, L. W. In *Handbook of Conducting Polymers*; Skotheim, T. A., Ed.; Dekker: New York, 1986; Vol. 1, pp 213–264. (b) Naarmann, R. In *Conjugated Polymeric Materials: Opportunities in Electronics, Optoelectronics, and Molecular Electronics*; Brédas, J. L., Chance, R. R., Eds.; Kluwer Academic: Dordrecht, The Netherlands, 1990; Vol. 182, pp 11–54. (c) Gorman, C. B.; Grubbs, R. H. In *Conjugated Polymers*; Brédas, J. L., Silbey, R., Eds.; Kluwer Academic: Dordrecht, The Netherlands, 1991; pp 1–48.
(2) Gin, D. L.; Conticello, V. P.; Grubbs, R. H. *Polym. Mater. Sci. Eng.* **1992**, *67*, 87.
(3) Ivory, D. M.; Miller, G. G.; Sowa, J. M.; Shacklette, L. W.; Chance, R. R.; Baughman, R. H. *J. Chem. Phys.* **1979**, *71*, 1506.
(4) Delugeard, Y.; Desuche, J.; Baudour, J. L. *Acta Crystallogr., Sect. B* **1976**, *32*, 702.
(5) Baudour, J. L.; Cailleau, H.; Yelon, W. B. *Acta Crystallogr., Sect. B* **1977**, *32*, 1773.
(6) Baudour, J. L.; Delugeard, Y.; Rivet, P. *Acta Crystallogr., Sect. B* **1978**, *34*, 625.
(7) Shacklette, L. W.; Chance, R. R.; Ivory, D. M.; Miller, G. G.; Baughman, R. H. *Synth. Met.* **1979**, *1*, 307.
(8) Zannonni, G.; Zerbi, G. *J. Chem. Phys.* **1985**, *82*, 31.
(9) Lefrant, S.; Buisson, J. P. In *Organic Molecules for Nonlinear Optics and Photonics*; Kluwer Academic: Dordrecht, The Netherlands, 1991; p 313.
(10) Buisson, J. P.; Krichēne, S.; Lefrant, S. *Synth. Met.* **1987**, *21*, 229.
(11) Pelous, Y.; Froyer, G.; Herold, C.; Lefrant, S. *Synth. Met.* **1989**, *29*, E17.
(12) Furukawa, Y.; Ohta, H.; Sakamoto, A.; Tasumi, M. *Spectrochim. Acta* **1991**, *47A*, 1367.
(13) Cui, C. X.; Kertesz, M. *J. Chem. Phys.* **1990**, *93*, 5257.
(14) Cui, C. X.; Kertesz, M.; Dupuis, M. *J. Chem. Phys.* **1990**, *93*, 5890.
(15) Cui, C. X.; Kertesz, M. *Macromolecules* **1992**, *25*, 1103.
(16) (a) Cui, C. X.; Kertesz, M.; Eckhart, H. *Synth. Met.* **1991**, *41–43*, 3491. (b) Eckhardt, H.; Baughman, R. H.; Buisson, J. P.; Lefrant, S.; Cui, C. X.; Kertesz, M. *Synth. Met.* **1991**, *43*, 3413.
(17) Painter, P. C.; Coleman, M. M.; Koenig, J. L. *The Theory of Vibrational Spectroscopy and Its Application to Polymers*; Wiley: New York, 1982.
(18) Frisch, M. J.; Head-Gordon, M.; Trucks, G. W.; Foresman, J. B.; Schlegel, H. B.; Raghavachari, K.; Robb, M.; Binkley, J. S.; Gonzalez, C.; Defrees, D. J.; Fox, D. J.; Whiteside, R. A.; Seeger, R.; Melius, C. F.; Baker, J.; Martin, R. L.; Kahn, L. R.; Stewart, J. J. P.; Topiol, S.; Pople, J. A. Gaussian, Inc., Pittsburgh, PA, 1990.
(19) Frisch, M. J.; Head-Gordon, M.; Trucks, G. W.; Head-Gordon, M.; Gill, P. M. W.; Wong, M. W.; Foresman, J. B.; Johnson, B. G.; Schlegel, H. B.; Robb, M. A.; Replogle, E. S.; Gomperts, R.; Andres, J. L.; Raghavachari, K.; Binkley, J. S.; Gonzalez, C.; Martin, R. L.; Fox, D. J.; Defrees, D. J.; Baker, J.; Stewart, J. J. P.; Pople, J. A. Gaussian, Inc., Pittsburgh, PA, 1992.
(20) Pulay, P.; Fogarasi, G.; Boggs, J. E.; Vargha, A. *J. Am. Chem. Soc.* **1983**, *105*, 7037.
(21) Pulay, P.; Fogarasi, G.; Boggs, J. E. *J. Chem. Phys.* **1981**, *74*, 3999.
(22) (a) Szalay, P. G.; Karpfen, A.; Lischka, H. J. *J. Chem. Phys.* **1987**, *87*, 3530. (b) Bock, C. W.; Panchenko, Y. N.; Pupyshev, V. I. *J. Comput. Chem.* **1990**, *11*, 623. (c) Guo, H.; Karplus, M. *J. Chem. Phys.* **1991**, *44*, 3679. (d) Kofranek, M.; Lischka, H.; Karpfen, A. *J. Chem. Phys.* **1992**, *96*, 982.
(23) Charbonneau, G. P.; Delugeard, Y. *Acta Crystallogr., Sect. B* **1976**, *32*, 1420.
(24) Charbonneau, G. P.; Delugeard, Y. *Acta Crystallogr., Sect. B* **1977**, *33*, 1586.
(25) Almenningen, A.; Bastiansen, O.; Fernholt, L.; Cyvin, B. N.; Cyvin, S. J.; Samdal, S. *J. Mol. Struct.* **1985**, *128*, 59.
(26) Tinland, B. *Acta Phys. Acad. Sci. Hung.* **1968**, *25*, 111.
(27) Zerbi, G.; Sandroni, S. *Spectrochim. Acta* **1967**, *24A*, 483.
(28) Barrett, R. M.; Steele, D. *J. Mol. Struct.* **1971**, *11*, 105.
(29) Kofranek, M.; Kovář, T.; Lischka, H.; Karpfen, A. *J. Mol. Struct.* **1992**, *259*, 181.
(30) Kofranek, M.; Kovář, T.; Karpfen, A.; Lischka, H. *J. Chem. Phys.* **1992**, *96*, 4464.
(31) Krichene, S. Ph.D. Thesis, Université de Nantes, Nantes, France, 1986; p 77.
(32) Božović, I.; Raković, D. *Phys. Rev.* **1985**, *B32*, 4235.
(33) Krichene, S.; Buisson, J. P.; Lefrant, S. *Synth. Met.* **1987**, *17*, 589.
(34) Carreira, L. A.; Towns, T. G. *J. Mol. Struct.* **1977**, *41*, 1.
(35) Fauvarque, J. F.; Jin, C. Q.; Petil, M. A.; Savard, J. *Makromol. Chem.* **1985**, *186*, 2415.
(36) (a) Kuzmany, H.; Imhoff, A.; Fitchen, D. B.; Sarhangi, A. *Phys. Rev. B.* **1982**, *26*, 7109. (b) Kürti, J.; Kuzmany, H. *Phys. Rev. B* **1991**, *44*, 597. (c) Brivio, G. P.; Mulazzi, E. *Chem. Phys. Lett.* **1983**, *95*, 555. (d) Brivio, G. P.; Mulazzi, E. *Phys. Rev. B* **1983**, *95*, 555.
(37) (a) Horovitz, B. *Solid State Commun.* **1982**, *41*, 729. (b) Horovitz, B.; Ehrenfreund, E.; Brafman, O. *J. Phys. C: Solid State Phys.* **1986**, *19*, 7291. (c) Ehrenfreund, E.; Vardeny, Z.; Brafman, O.; Horovitz, B. *Phys. Rev. B* **1987**, *36*, 1535.
(38) (a) Zerbi, G.; Gussoni, M.; Castigiloni, C. In *Conjugated Polymers*; Bredas, J. L., Silbey, R., Eds.; Kluwer Academic: Dordrecht, The Netherlands, 1991; pp 435–507. (b) Zerbi, M.; Chierichetti, B. *J. Chem. Phys.* **1991**, *94*, 4637. (c) Castiglioni, C.; Gussoni, M.; Zerbi, G. *Synth. Met.* **1989**, *29*, E1.
(39) Schaffer, H. E.; Chance, R. R.; Silbey, R. J.; Knoll, K.; Schrock, R. R. *J. Chem. Phys.* **1991**, *94*, 4161.
(40) Snyder, R. G. *J. Am. Chem. Soc.* **1990**, *23*, 2081.
(41) Zerbi, G.; Chierichetti, B.; Ingänas, O. *J. Chem. Phys.* **1991**, *94*, 4646.
(42) Cuff, L.; Cui, C.; Kertesz, M. To be published.